THEORETICAL AND EXPERIMENTAL DETERMINATION OF THE FLAME TRANSFER FUNCTION OF CONFINED PREMIXED CONICAL FLAMES

A. Cuquel *, D. Durox * and T. Schuller *
alexis.cuquel@em2c.ecp.fr
* Laboratoire EM2C, CNRS and Ecole Centrale Paris, 92295 Châtenay-Malabry, France.

Abstract
The response of conical premixed flames to velocity perturbations is examined for different flow operating conditions, different burner nozzle geometries with and without flame tube to confine the reaction zone. The study focuses on the type of flow perturbations to consider in order to reproduce the correct gain and phase of the flame transfer function (FTF). In all cases explored, it is shown that only a convective model considering a divergence free perturbed velocity field enables to reproduce the phase of the FTF. In this model, flow perturbations are convected by the mean flow and are locally incompressible. Theoretical predictions are compared to experimental results. A specific focus is given on the effect of confinement on the flame response by measuring the spatial evolution of the velocity field in the fresh gases stream. This is used to highlight the limits of the model, and to identify further requirements one should consider to improve the modeling of the FTF gain. The model proposed may be used to improve predictions of thermo-acoustic instabilities by a better description of the phase of the flame response.

Introduction
Premixed systems often feature acoustically coupled instabilities which reduce their domain of operation and have many detrimental effects [1, 2]. The prediction of these undesirable regimes requires a detailed knowledge of the combustor acoustics and the flame response to flow perturbations which is difficult to describe. Low-order thermo-acoustic models then often relies on the knowledge of the Flame Transfer Function (FTF) linking incoming flow perturbations to heat release rate disturbances and predictions improve with a better description of the FTF [3, 4, 5]. In perfectly premixed systems and in absence of mixture composition disturbances, the flame responds to velocity perturbations [6]. In the limit of small perturbations [7], it is defined in terms of a gain G and a phase φ, both function of the angular frequency ω :

$$F(\omega) = \frac{\widetilde{\dot{Q}}_1/\dot{Q}_0}{v_1/v_0} = G(\omega)e^{i\varphi(\omega)} \tag{1}$$

where fluctuations are analyzed in the frequency space by expanding the flow variables as $a = a_0 + \tilde{a}_1 \exp(-i\omega t)$, $\widetilde{\dot{Q}}_1$ and v_1 indicating fluctuations in heat release rate and velocity at the burner outlet respectively.

The case of conical flames constitutes one interesting generic configuration where it is possible to obtain an analytical expression for this FTF [8, 9, 10, 11]. This can be used to identify the main parameters controlling the flame response [6, 12, 13, 14, 15, 16], or validate simulations tools [17, 18]. Many different models have been proposed including effects of the flow velocity, stretch and curvature effects [19], anchoring point dynamics [20] but a few were validated yet against detailed measurements of the FTF [9, 10, 13]. This work aims at identifying the main flow parameters controlling the response of conical

flames submitted to velocity modulations when the burner geometry is modified, the flow operating conditions are changed and the flame is confined. It is shown that the main features of the flame response can be reproduced by including a better description of the perturbed velocity field, a problem which has not been envisaged yet in previous modeling and strongly modify the flame response.

The analysis relies on the level set description of the flame front displacement:

$$\frac{\partial G}{\partial t} + \mathbf{v} \cdot \nabla G = S_L |\nabla G| \tag{2}$$

where $\mathbf{v}$ indicates the flow velocity at the flame front location and S_L denotes the laminar burning speed with respect to the fresh mixture. In the case of a uniform mean axial flow $\mathbf{v} = v_0 \mathbf{e}_y$, this equation reduces in a reference frame attached to the steady flame inclined with an angle α with respect to the axial direction $\mathbf{e}_y$ [10] to:

$$\frac{\partial \xi}{\partial t} + \overline{U} \frac{\partial \xi}{\partial X} = V'(X,t) \tag{3}$$

where $\overline{U} = v_0 \cos\alpha$ denotes the mean flow velocity component tangential to the flame front, $V'(X,t)$ corresponds to the velocity perturbation normal to the steady flame front, evaluated at the steady flame front position, and ξ is the flame front displacement normal to its steady position.

One of the difficulty is to accurately model the velocity perturbation $V'(X,t)$ impinging the flame front. In most studies a uniform flow perturbation from the burner outlet is considered by invoking that the acoustic disturbance wavelengths are large compared to the flame size [8, 9, 12, 20]. In this case $V'(X,t) = \tilde{V}_1 \exp(-i\omega t)$ is only a function of time and is given by $\tilde{V}_1 = v_1 \sin\alpha$. In the comparisons with experimental data conducted in [9], this type of perturbation was considered and this model was shown to well reproduce the gain, as well as the phase in the very low frequency range. The phase predictions however rapidly deviate from measurements at higher frequencies where the phase of the model saturates around $\pi/2$ while experimental data still feature a regular increase in this frequency range. Later, stretch and curvature effects were shown to only barely modify the flame response and cannot explain such behavior [19]. It was demonstrated by [12] that flame front wrinkles are convected along the flame front in a perturbed flow confirming earlier observations [21]. This was used by Baillot *et al.* [13, 22] to analyze cusp formation along the flame front and identify a convected wave in the velocity field of pulsated conical flames. This type of convective perturbation has been considered in [10] to model the flame transfer function. In this case the velocity perturbation writes $\tilde{V}_1 = v_1 \sin\alpha \exp(iky)$, where $k = \omega/v_0$ is a convective wavenumber along the burner axis y. This model barely modifies the gain of the FTF. It succeeded in predicting correctly the slope of the phase of the FTF at high frequencies, but was mismatching at very low frequencies. One of the weakness of this model is to violate continuity. A convective model satisfying mass balance has been proposed in [13] and used to retrieved the flame front deformations at specific frequencies, but the FTF was not determined in this study. It was shown by numerical integration of the G- equation [17] that this type of perturbed flow field enables to retrieve the low and high frequency behavior of the FTF. There has been yet no attempt to develop an analytical description for the FTF including this type of perturbation.

Predictions of unstable operating modes remain difficult with previous analytical descriptions since the phase of the FTF, mainly determining the stability of the system [23], is not well reproduced. Collections of small conical flames are often used in practice and feature a complex response which is generally determined experimentally [5, 7, 24]. There are also a few attempts where the response is modeled using the FTF of a unique conical

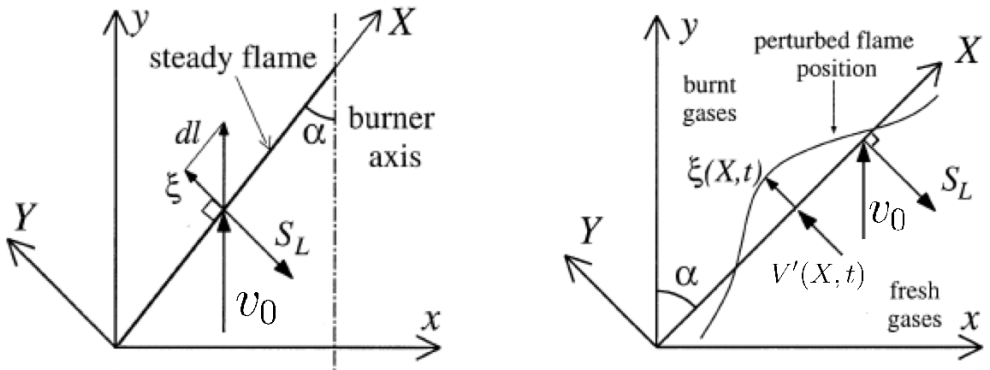

Figure 1. : Schematic representation of an inclined flame sheet with an angle α characterized by a displacement speed S_L in a uniform mean axial flow v_0 submitted to velocity perturbations. The flame front normal displacement ξ is due to the normal velocity perturbation $V'(X,t)$ in the flame reference frame (X,Y).

flame [20, 25]. Some numerical investigations show however that the effect of the flame confinement is essential to model these systems [26]. Before envisaging more sophisticated configurations, it is important to obtain an accurate description of the response to flow perturbations of a single flame, with or without confinement.

In the present work, a convective perturbation in the fresh gases satisfying the continuity equation is used to determine the FTF of conical flames submitted to harmonic velocity modulations. An analytical expression is obtained in section 2. This flame response is compared to previous models [9, 10] and a low frequency approximation is derived to show that it reduces to previous uniform model predictions at low frequencies. An experimental validation is then conducted with the setup described in section 3. Measurements of the FTF are presented for different burner geometries and flow conditions. These data includes a focus on effects of confinement on the flame response that are completed by a characterization of the spatial evolution of the velocity field along the burner centerline. A discussion is developed in section 4 to examine the limits of the proposed model and to identify further developments that need to be considered.

1 Theoretical developement

Incompressible convective velocity model

The case of premixed flame stabilized on an axisymmetric burner with a nozzle diameter R is considered when the flow is uniform at the burner outlet. The flame that takes a conical shape is submitted to acoustic modulations. The flame front wrinkles due to the velocity perturbation in the fresh gases stream, acting as a forcing term in the G-equation, and the convection of these deformations along the steady flame front takes place at a velocity equal to $v_0 \cos\alpha$. The perturbed flow in the vicinity of the flame can locally be treated as incompressible as long as the acoustic disturbance wavelength remains large compared to the flame height [14]. The perturbed flow field considered comprises then a convected wave but should remain divergence free. In the burner frame (x, y), it takes the following form :

$$\widetilde{u}_1 = ik\frac{(R-x)}{2}v_1 \exp(iky) \quad (4)$$

$$\widetilde{v}_1 = v_1 \exp(iky) \quad (5)$$

where v_1 denotes the amplitude of the axial velocity perturbation at the burner outlet $y = 0$. The radial perturbation u'_1 vanishes on the burner centerline and both axial v'_1 and radial u'_1 disturbances are convected by the uniform axial mean flow ($u_0 = 0, v_0 = cte$) with a wavenumber $k = \omega/v_0$ based on the mean flow velocity u_0 along the axial direction $\mathbf{e}_y$. The corresponding velocity perturbation normal to the steady flame front and evaluated at the steady flame front location writes in this case:

$$\tilde{V}(X, Y = 0) = v_1 \sin\alpha \left[1 - i\frac{1}{2}k_* \left(1 - \frac{X \sin\alpha}{R}\right)\right] \exp\left(ik_* \frac{X \sin\alpha}{R}\right) \tag{6}$$

where $k_* = \omega_* \cos^2\alpha$ is a dimensionless flow wavenumber based on flow perturbations propagating at a velocity v_0 along the axial direction over a distance equal to the flame height H, and $\omega_* = \omega R/(S_L \cos\alpha)$ is a dimensionless flame wavenumber related to flame front deformations propagating at a speed $v_0 \cos\alpha$ along the flame front over a distance corresponding to the flame front length L :

$$k_* = \omega_* \cos^2\alpha = \frac{\omega}{v_0} H \tag{7}$$

$$\omega_* = \frac{\omega R}{S_L \cos\alpha} = \frac{\omega}{v_0 \cos\alpha} L \tag{8}$$

Integration of Eq. (3) with the flow perturbation Eq. (6) leads to the following expression for the the flame front displacement:

$$\frac{\tilde{\xi}(u)\cos\alpha}{R} = \frac{v_1}{v_0}\frac{1}{i(k_* - \omega_*)} \cdot \left[\left(1 - i\frac{1}{2}k_* - \frac{1}{2}\frac{k_*}{k_* - \omega_*}\right)(\exp(ik_*u) - \exp(i\omega_*u)) - i\frac{1}{2}k_* u \exp(ik_*u)\right] \tag{9}$$

where $u = X/L$ is the dimensionless space variable along the steady flame front featuring a length L. This equation is then integrated over the flame length L to obtain an expression for the relative perturbations in flame surface area $A' = \tilde{A}_1 \exp(-i\omega t)$ corresponding also to heat release rate disturbances in absence of mixture composition inhomogeneities:

$$\frac{\widetilde{\dot{Q}}_1}{\dot{Q}_0} = \frac{\tilde{A}_1}{A_0} = \frac{v_1}{v_0} F_A \tag{10}$$

where the Flame Transfer Function F_A is given by :

$$F_A = \frac{1}{i(k_* - \omega_*)} \cdot \left[2\left(1 - i\frac{1}{2}k_* - \frac{1}{2}\frac{k_*}{k_* - \omega_*}\right)\left(\frac{\exp(ik_*) - 1}{ik_*} - \frac{\exp(i\omega_*) - 1}{i\omega_*}\right) + \left(\exp(ik_*) - \frac{\exp(ik_*) - 1}{ik_*}\right)\right] \tag{11}$$

An example for the gain and phase of F_A for a conical flame with an angle $\alpha = 0.3$ rad (i.e. with $v_0 = 1.32$ m.s^{-1} and $S_L = 0.4$ m.s^{-1}) is plotted in Fig. 1 as a function of the reduced frequency ω_*. Results are compared to predictions with a uniform model F_U (dashed-dotted lines) [9] and with a convective wave F_C (dashed lines) [10], given by:

$$F_U = \frac{2}{\omega_*^2}\left[1 - \exp(i\omega_*) + i\omega_*\right] \tag{12}$$

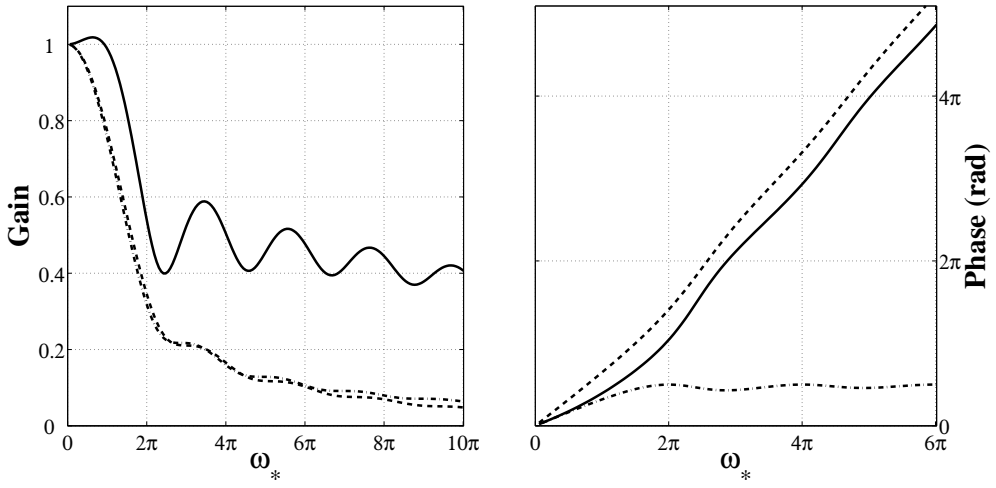

Figure 2. : Gain (left) and phase (right) of the FTF for a flame angle $\alpha = 0.3$ rad as a function of the reduced frequency ω_*. Solid line : F_A (convective wave satisfying continuity). Dashed-dotted line : F_U (uniform flow perturbation [9]). Dashed lines : F_C (convective wave [10]).

$$F_C = \frac{2}{i(k_* - \omega_*)} \left[\frac{\exp(ik_*) - 1}{ik_*} - \frac{\exp(i\omega_*) - 1}{i\omega_*} \right] \tag{13}$$

The gain is larger than the previous models but it features also higher amplitude oscillations. The phase now collapses with estimates obtained with bulk flow modulations at low frequencies (dashed-dotted lines) and features the correct asymptotic behavior at higher frequencies already identified with the convective model (dashed lines). It is interesting to further analyze the low frequency behavior.

Low frequency phase behavior

One difficulty with the convective model developed in [10] is the poor agreement with experimental data at low frequencies. As mentioned previously, the theoretical expression F_U derived in [9] reproduces well experimental data in the low frequency limit, while the model F_C developed in [10] was shown to over-predict the phase in this frequency range. The new model developed herein is expected to improve results in the low-frequency range by locally satisfying mass balance [17]. These different models are compared under the assumption $\omega_* \ll 1$. A development in Taylor series around the value $\omega_* = 0^+$ yields:

$$F_U \underset{0^+}{\sim} 1 + \frac{i\omega_*}{3} \qquad F_C \underset{0^+}{\sim} 1 + \frac{i\omega_*}{3}(1 + \cos^2\alpha) \qquad F_A \underset{0^+}{\sim} 1 + \frac{i\omega_*}{3} \tag{14}$$

The first two expressions obtained in [9, 10] show the incompatibility of the uniform and convective models at low frequencies. This leads to an over-prediction with the convective model, while the new model now reaches the correct low frequency limit and also conserve a convective pattern which is observed experimentally in the upper frequency range for small perturbation levels [7, 16].

2 Experimental validation

Experimental setup

The configuration studied here is presented in Fig. 3. This burner is used to stabilized perfectly premixed methane-air flames at different equivalence ratios. The burner is fed from the bottom into a cylindrical feeding manifold. It is also equipped with a honeycomb,

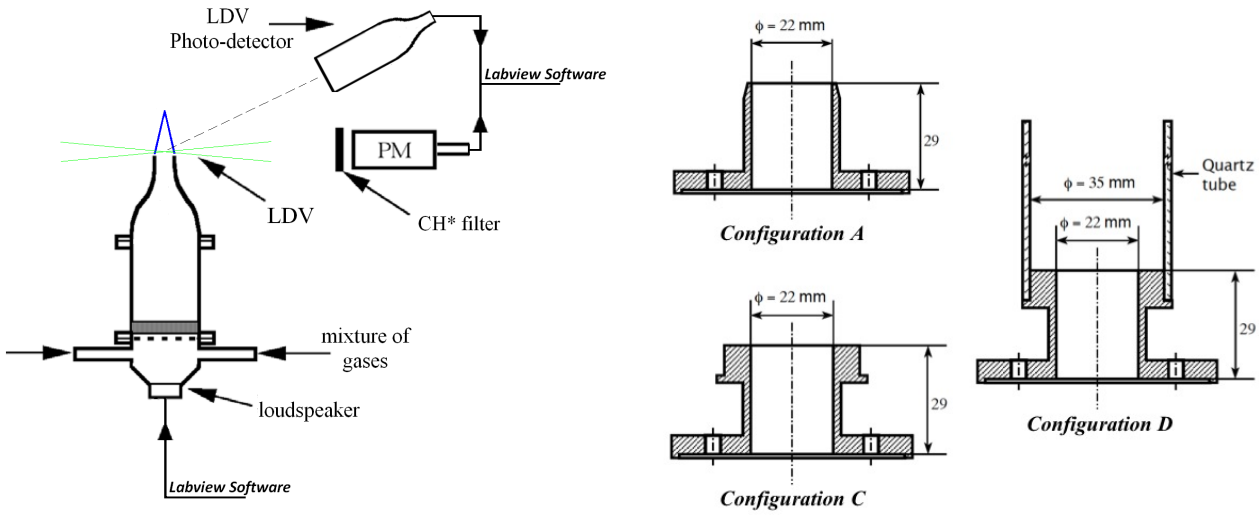

Figure 3. : Experimental setup with the diagnostic equipment (left figure) and the detailed burner exits (right figure).

a laminarization grid and a convergent nozzle to obtain a laminar top-hat velocity profile at the circular nozzle exit. A loudspeaker is mounted at the bottom of the burner to generate acoustic perturbations which modulates the flow at the burner exit.

The burner can be equipped with three different nozzle outlets. The two first correspond to cylindrical pieces with a 1 mm-wide beveled edge. Burner A has a radius $R = 11$ mm and burner B features a larger radius $R = 15$ mm. The last nozzle is a cylindrical piece that comprises an external plateau. Burner C has an internal outlet radius $R = 11$ mm and thickness $l = 6.5$ mm at the outlet section. This nozzle can also be equipped with a quartz confinement tube of radius $r = 17.5$ mm and length $l = 100$ mm to explore effects of lateral confinement on the flame response. It is further referenced as burner D. Two flow mass meters were used to control both the equivalence ratio and the bulk velocity at the burner outlet. Flames at three different equivalence ratios were investigated: $\phi = 0.8$, 1.0 and 1.1 corresponding to laminar burning velocities $S_L = 0.29$, 0.39 and 0.39 m.s^{-1}. Experiments were all conducted for a small input level to remain in the linear regime by keeping the relative velocity perturbation level constant at the burner outlet $v_1^{rms}/v_0 = 0.05$ except in Fig. 6 where the fluctuation level was increased to $v_1^{rms}/v_0 = 0.10$.

The loudspeaker was driven by a harmonic signal through a function generator and an amplifier, so that the acoustic velocity perturbation level and frequency can be easily swept. The heat release rate was measured with a photodiode (PM) equipped with a OH* filter by collecting the chemiluminescence emission from the flame. The velocity was measured by Laser Doppler Velocimetry (LDV) with a data acquisition rate of 16,384 Hz. The burner was mounted on a micrometric sliding rail enabling measurements of the velocity field along the burner axis, from 1.24 mm above the burner exit to the tip of the flame. The signals were recorded with a National Instrument analog-to-digital converter board controlled by the LabVIEW software, at a sampling frequency of 32,768 Hz. This software was also used to post-process the time series recorded by the different sensors and to compute the FTF presented hereafter using a Welch periodogram method to improve the signal to noise ratio.

Results on the beveled edge burner

Results presented in Fig. 4 are gain and phase of conical flames anchored on burners A and B featuring beveled edges for different flow parameters and different outlet radius.

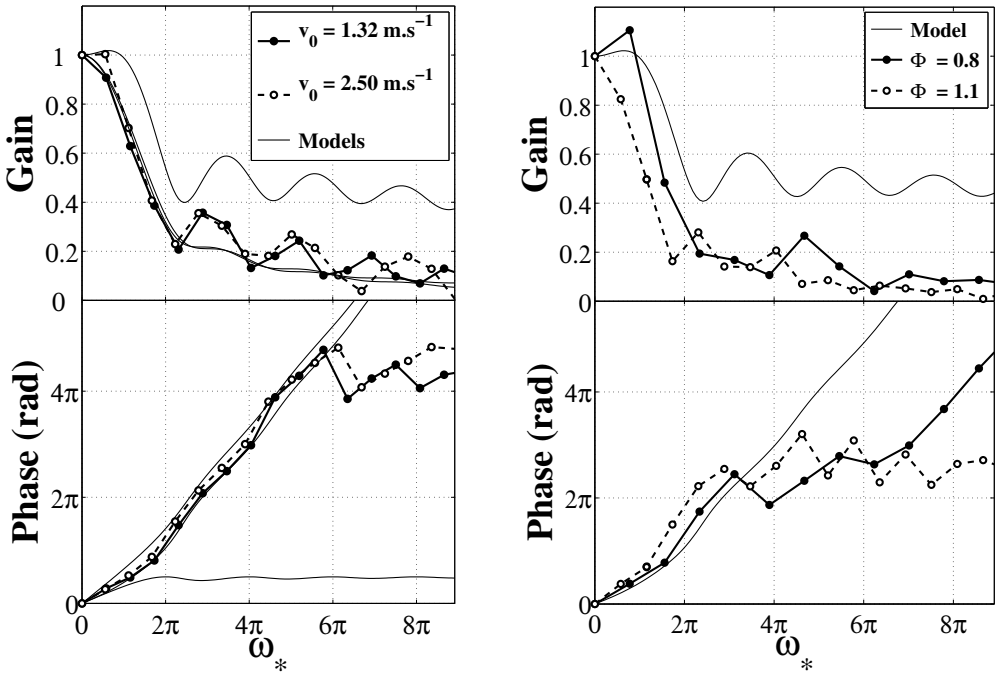

Figure 4. : Gain and phase of the FTF for burners A (left) and B (right) featuring beveled edges and different outlet radius. $\phi = 1.1$ and $R = 11$ mm (left figure), and $v_0 = 1.30$ m.s^{-1} and $R = 15$ mm (right figure). Experimental data are also compared to predictions with F_A, and also with F_U (uniform velocity perturbations) and F_C (convective velocity perturbations) in the left figure.

In these experiments, the height of the steady flame has been modified, either through a change in the bulk velocity or burning velocity.

In the left figure, the bulk velocity is the varying parameter, while the equivalence ratio $\phi = 1.1$ and the burner radius $R = 11$ mm were kept constant. In the right figure, the equivalence ratio was changed corresponding to different flame speeds while the bulk velocity $v_0 = 1.30$ m.s^{-1} and the burner radius $R = 15$ mm were kept constant. Results are plotted as function of the reduced frequency $\omega_* = \omega R/(S_L \cos\alpha)$. The experimental curves exhibit a good match at low frequencies indicating that ω_* is the right dimensionless number to characterize the FTF in the low frequency range. A slight drift between the curves is observed in the upper frequency range though. The new model presented in this article exhibits an excellent match for the phase behavior except at very high frequencies where the phase saturates. The gain is slightly over-predicted but its evolution and the location of secondary extrema are correctly retrieved by the model. Predictions obtained with the previous models F_U and F_C are also plotted on this figure. The improvement on the phase prediction in the low frequency range is obvious. As for the gain, the previous models led to good approximations of its magnitude, but the new model definitely shows the right trends and oscillations, even if they are over-predicted.

In the right figure, the equivalence ratio was changed from $\phi = 0.8$ to $\phi = 1.1$ corresponding to different burning velocities, $S_L = 0.29$ m.s^{-1} and $S_L = 0.39$ m.s^{-1} respectively. Results obtained for the rich mixture cases show the same type of behavior as in the left figure. The phase seems to saturate earlier, but a better frequency resolution would be needed to give a definite evidence. Again, the modeled phase matches well with experiments at $\phi = 1.1$ in the low frequency range and miss the phase saturation around 4π. The gain is over-predicted but exhibits the good trends. Experimental data

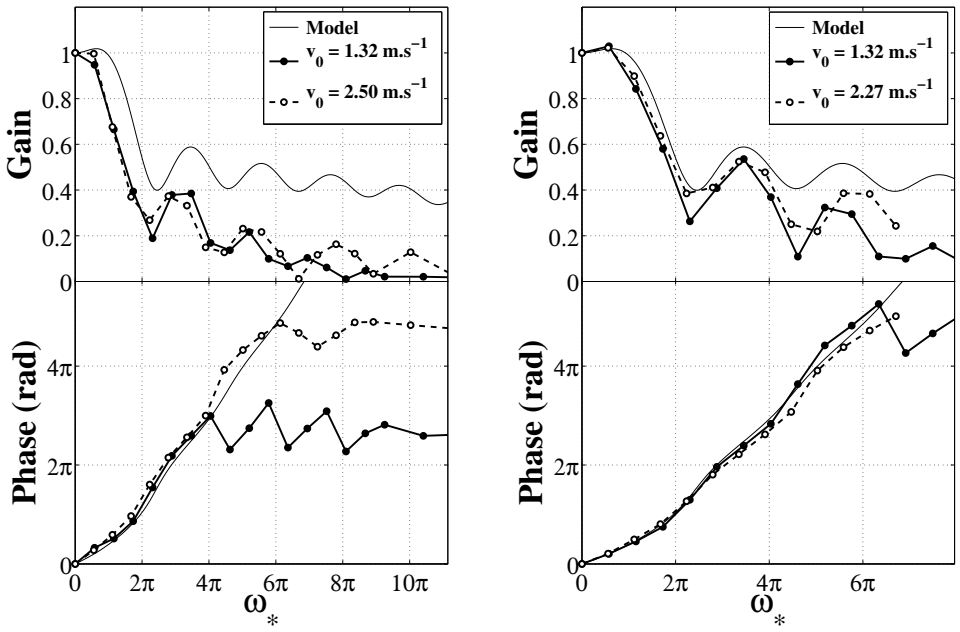

Figure 5. : Gain and phase of the FTF for burners C (without flame tube - left figure) and D (with flame tube - right figure) featuring a thick plateau and a nozzle outlet radius $R = 11$ mm. Experimental data presented for different flow velocities (symbols) are compared to predictions with F_A (solid line).

obtained for $\phi = 0.8$ indicate a different trend with a slight drift between predictions and measurements for the phase with respect to ω_* that only collapse at very low frequencies. The general regular increase of the phase is however retrieved and a gain exceeding unity at very low frequencies is also observed as in the predictions. This characteristic is absent in the rich case explored.

We can then conclude that the burning velocity has a much bigger influence on the flame response than the bulk flow velocity in the cases considered here. This is probably the result of the little dependance of ω_* on v_0 for elongated flames, for which $\cos\alpha \simeq 1$. The burning velocity S_L also appears in the expression of ω_*. A slight error in this quantity has a larger impact on the results. It has been shown that by matching the steady flame height with experiments, the FTF collapse to experimental results [17]. The correct quantity appearing in ω_* is indeed the flame displacement speed S_d that can related to the experimentally determined flame height such as :

$$S_d = v_0 \sin\alpha_{exp} \qquad \text{where} \qquad \alpha_{exp} = \arctan(\frac{R}{H_{exp}}) \tag{15}$$

Effects of burner edges and confinement

The response of conical flames stabilized on a burner featuring a thick plateau at the outlet is examined when the flame is confined by a quartz tube or free to expand. Results are shown in Fig. 5 without flame tube (left figure) and with flame tube (right figure). In the absence of flame tube, experimental data obtained for burner C at two different flow velocities $v_0 = 1.32$ and 2.50 m.s^{-1} and a mixture equivalence ratio $\phi = 1.1$ again collapse when plotted as function of the reduced frequency ω_*. The gain shows little dependance on the bulk velocity, except at high frequencies where a mismatch in the minima locations is observed between the two sets of data. This feature was also observed previously for the beveled edge burner equipped with thin edges. The phase also collapses up to reduce

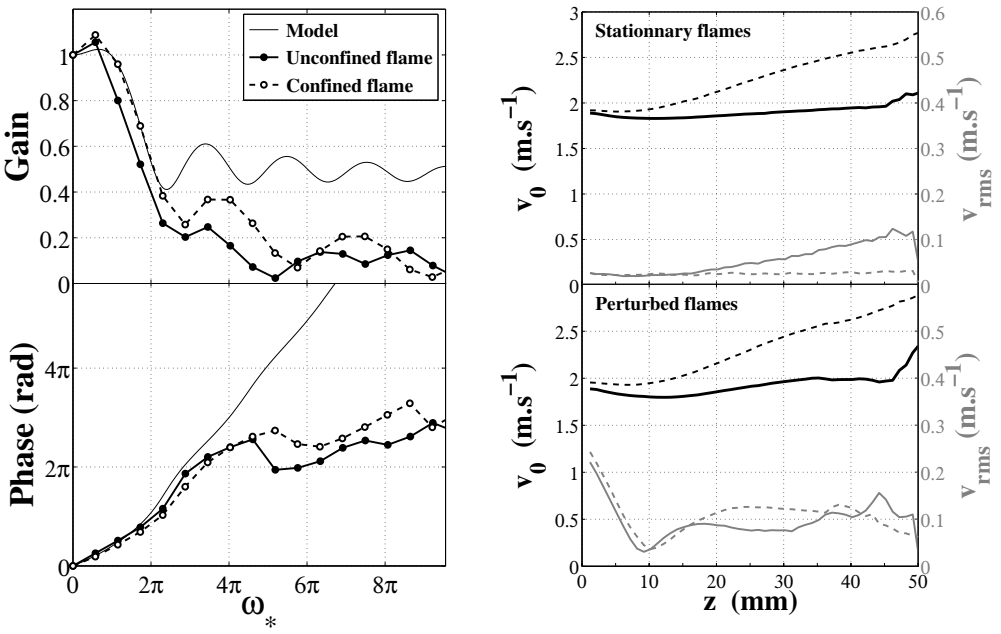

Figure 6. : Left figure : Comparison between the FTF with and without flame tube for $v_0 = 1.89$ m.s^{-1}, $\phi = 1.0$ and $v_1^{rms}/v_0 = 0.10$. Right figure : axial velocity components along the burner axis : mean velocity $v_0(z)$ (black) and fluctuating velocity $v_1^{rms}(z)$ (grey) in steady (upper figure) and perturbed conditions at 100 Hz (lower figure). With flame tube (dashed lines). Without flame tube (solid line).

frequencies $\omega_* = 4\pi$ and then a difference in the saturation is observed. The model catches well the phase evolution except the saturation of the phase at high frequencies and the gain is again slightly over-predicted. This shows that the flame response is not sensitive to the type of rim used to anchor the flame. When the flame is confined with burner D, the flame responses again collapse as a function of ω_* for the two flow velocities investigated $v_0 = 1.32$ and 2.27 m.s^{-1} at the same mixture composition $\phi = 1.1$. The only difference observed is an increased gain compared to the unconfined cases presented in the left figure. Model predictions now greatly improves the phase as well as the gain of the FTF over a large frequency range except at very high frequencies where the gain is overestimated.

Differences observed between the confined and the unconfined flame responses are further investigated by examining the evolution of the axial velocity along the burner axis. Results are presented in Fig. 6 for slightly different operating conditions $v_0 = 1.89$ m.s^{-1}, $\phi = 1.1$ and $v'/v_0 = 0.10$. For this input level, the gain of the FTF decreases slightly compared to data obtained at a lower modulation level. Increasing the input level is known to reduce the gain. The phase is also seen to saturate at lower frequencies as well [7, 16]. Velocity measurements were first done in absence of modulation (upper figure) and when the flow is modulated at 100 Hz (lower figure). The evolution of the mean $v_0(z)$ (black curves) and r.m.s. fluctuating $v_1^{rms}(z)$ (grey curves) velocity components are presented for the confined flame (dashed lines) and the unconfined flame (solid line). In absence of flow perturbation, the mean axial velocity remains uniform and r.m.s fluctuation are vanishing. The r.m.s value is slightly increasing for large z because of the flickering of the flame tip. The main differences observed with confinement is the regular increase of the mean axial velocity along the burner axis, and the suppression of the r.m.s fluctuations due to flickering. When the flame is modulated at 100 Hz, the mean axial velocity components are not affected by the perturbation and remain close to the steady profiles.

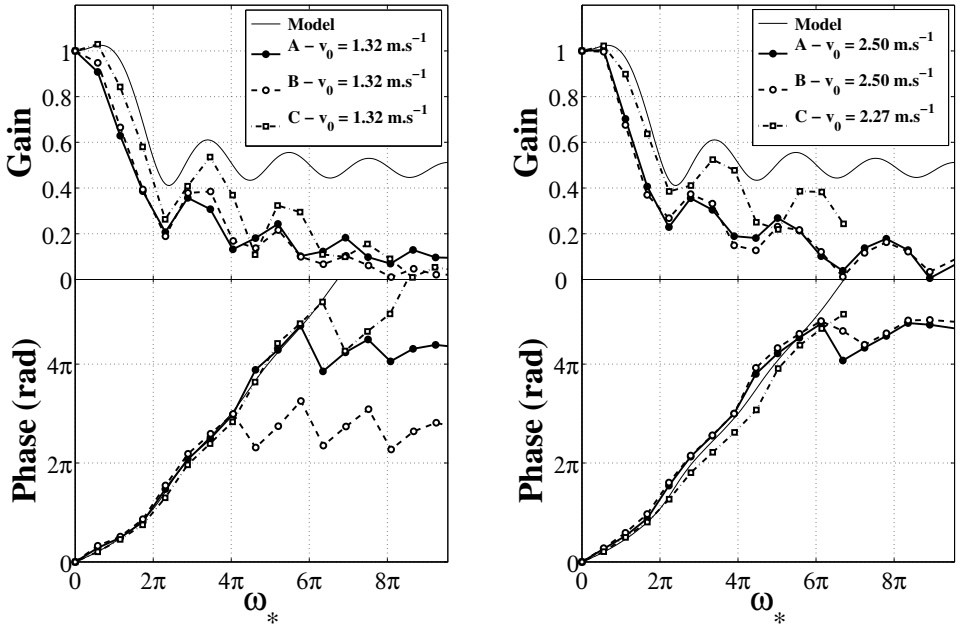

Figure 7. : Comparison of the influence of the burner exit geometry on the CFTF, for three different geometries : A - Beveled-edge burner; C - Unconfined plateau-shaped burner exit; D - Confined plateau-shaped burner exit, for two different bulk velocities : $v_0 = 1.32$ m.s^{-1} and $v_0 = 2.27/2.50$ m.s^{-1}.

The mean axial velocity field remains uniform in absence of flame tube while it increases regularly with the flame tube. This contrasts with the perturbed velocity field which is less affected by flame confinement. The r.m.s velocity evolution indicates that the amplitude of velocity perturbations rapidly decreases with the distance y from the burner exit and then reaches a constant value at half the r.m.s value of the amplitude imposed at the burner exit [14]. These distinct phenomena, corresponding to an increase of the mean velocity induced by the confinement, and a drop of the r.m.s velocity fluctuation along the burner axis are not included in the models. They compete and may be used to explain the different evolutions observed in the gain.

3 Discussion

When the mean flow velocity is increased due to the confinement, this leads to longer flames with increased flame surface area fluctuations and higher values of the FTF gain. This is confirmed by the evolution of the flame height that can be identified in the steady and perturbed velocity profiles in absence of flame tube around $z = 45$ mm when the velocity increases suddenly due to the flickering in Fig. 6. This sudden velocity increase cannot be detected in data with the flame tube meaning that the flame height is significantly higher. This simple argument shows that confined conical flames feature larger gains than unconfined flames for the same flow operating conditions and this is confirmed by experimental observations. The gain may also be affected by the decrease of the r.m.s perturbation level with the axial distance to the burner. This corresponds to lower flame surface area fluctuations compared to a uniform excitation along the flame front and a drop in the gain of the FTF. It is also known that this velocity drop increases with frequency [14] leading to even smaller flame surface area fluctuations as the frequency is increased. This behavior may explain the different results obtained for the FTF in absence of flame tube where predictions slightly overestimate the gain because the perturbed flow is considered constant in the model developed in this study. This was also confirmed by

simulations [17]. In presence of flame tube, both effects compete to determine the value of the gain but the flow acceleration due to confinement rapidly dominates.

A synthesis of the main results is presented in Fig. 7. The FTF for two different bulk velocities and three burner configurations are plotted against ω_*. Results in absence of flame tube are very close, except at high frequencies where the saturation level differs for the phase. The response features the same phase behavior but a significantly larger gain when it is confined in a flame tube. Minima in the gain are also located at slightly larger reduced frequencies ω_*. This is due to the larger flame height when it is confined. In this case the height is not given by $H = R\,\mathrm{cotan}(\arcsin(S_L/v_0))$ and the reduced frequency must be modified.

The exploration of the velocity field in the fresh gases also revealed new dynamics that need to be included for further improvement. With flame tube, despite the good match between experimental and theoretical results, the investigation showed that the mean axial velocity increases with the distance to the burner. This may be included in future models for confined flames. Moreover, the amplitude of the axial velocity perturbation was shown to decrease along the burner axis with and without flame tube. This is certainly the key to fill the gap between experimental data and theoretical estimates of the gain which is systematically over-predicted in absence of flame tube. Finally, the saturation of the phase at high frequencies is still an open question. Several conjectures have been already proposed but no clear proof has been given yet on this topic.

4 Conclusion

The flame transfer function of conical pulsated flame has been studied both theoretically and experimentally. A new model for velocity perturbations which are convected by the mean flow has been introduced to satisfy the continuity equation in the fresh gases flow. An analytical expression for the FTF has been obtained with a phase that matches previous models at low and high frequencies. Comparisons with experimental data obtained for different nozzle geometries and flow operating conditions show a very good match of the phase which is an essential feature to reproduce in order to predict unstable regimes. It was also shown that this model over-predicts the gain in absence of flame tube but differences reduce when a flame tube is added. These comparisons have been conducted over a wide range of parameters, such as the bulk velocity, the equivalence ratio and the burner geometry.

References

[1] Candel, S., 2002. "Combustion dynamics and control: Progress and challenges". *Proceedings of the Combustion Institute,* ***29***(1), pp. 1–28.

[2] Lieuwen, T., and Yang, V., 2005. *Combustion instabilities in gas turbine engines: operational experience, fundamental mechanisms, and modeling.* American Institute of Aeronautics and Astronautics, Reston, VA, USA.

[3] Hubbard, S., and Dowling, A., 1998. "Acoustic instabilities in premix burners". In AIAA Paper 98-2272.

[4] Polifke, W., Poncet, A., Paschereit, C., and Doebbeling, K., 2001. "Reconstruction of acoustic transfer matrices by instationary computational fluid dynamics". *Journal of Sound and Vibration,* ***245***(3), pp. 483–510.

[5] Noiray, N., Durox, D., Schuller, T., and Candel, S., 2008. "A unified framework for nonlinear combustion instability analysis based on the flame describing function". *Journal of Fluid Mechanics,* ***615***(-1), pp. 139–167.

[6] Ducruix, S., Schuller, T., Durox, D., and Candel, S., 2003. "Combustion dynamics and instabilities: Elementary coupling and driving mechanisms". *J. Propul. Power,* ***19***, pp. 722–734.

[7] Durox, D., Schuller, T., Noiray, N., and Candel, S., 2009. "Experimental analysis of nonlinear flame transfer functions for different flame geometries". *Proceedings of the Combustion Institute,* ***32***(1), pp. 1391–1398.

[8] Fleifil, M., Annaswamy, A. M., Ghoneim, Z. A., and Ghoniem, A. F., 1996. "Response of a laminar premixed flame to flow oscillations: A kinematic model and thermoacoustic instability results". *Combustion and Flame,* ***106***(4), pp. 487–510.

[9] Ducruix, S., Durox, D., and Candel, S., 2000. "Theoretical and experimental determinations of the transfer function of a laminar premixed flame". *Proceedings of the Combustion Institute,* ***28***(1), pp. 765–773.

[10] Schuller, T., Durox, D., and Candel, S., 2003. "A unified model for the prediction of laminar flame transfer functions: comparisons between conical and v-flame dynamics". *Combustion and Flame,* ***134***(1-2), pp. 21–34.

[11] Lieuwen, T., 2005. "Nonlinear kinematic response of premixed flames to harmonic velocity disturbances". *Proceedings of the Combustion Institute,* ***30***(2), pp. 1725–1732.

[12] Boyer, L., and Quinard, J., 1990. "On the dynamics of anchored flames". *Combustion and Flame,* ***82***(1), pp. 51–65.

[13] Baillot, F., Durox, D., and Prud'homme, R., 1992. "Experimental and theoretical study of a premixed vibrating flame". *Combustion and Flame,* ***88***(2), pp. 149–152, IN1, 153–168.

[14] Birbaud, A., Durox, D., and Candel, S., 2006. "Upstream flow dynamics of a laminar premixed conical flame submitted to acoustic modulations". *Combustion and Flame,* ***146***(3), pp. 541–552.

[15] Kornilov, V., Schreel, K., and de Goey, L., 2007. "Experimental assessment of the acoustic response of laminar premixed bunsen flames". *Proceedings of the Combustion Institute,* ***31***(1), pp. 1239–1246.

[16] Karimi, N., Brear, M., Jin, S.-H., and Monty, J., 2009. "Linear and non-linear forced response of a conical, ducted, laminar premixed flame". *Combustion and Flame,* ***156***(11), pp. 2201–2212.

[17] Schuller, T., Ducruix, S., Durox, D., and Candel, S., 2002. "Modeling tools for the prediction of premixed flame transfer functions". *Proceedings of the Combustion Institute,* ***29***(1), pp. 107–113.

[18] Auzillon, P., Fiorina, B., Vicquelin, R., Darabiha, N., Gicquel, O., and Veynante, D., 2011. "Modeling chemical flame structure and combustion dynamics in les". *Proceedings of the Combustion Institute,* ***33***(1), pp. 1331–1338.

[19] Wang, H., Law, C., and Lieuwen, T., 2009. "Linear response of stretch-affected premixed flames to flow oscillations". *Combustion and Flame,* ***156***(4), pp. 889–895.

[20] Altay, H., Park, S., Wu, D., Wee, D., Annaswamy, A., and Ghoniem, A., 2009. "Modeling the dynamic response of a laminar perforated-plate stabilized flame". *Proceedings of the Combustion Institute,* ***32***(1), pp. 1359–1366.

[21] Petersen, R. E., and Emmons, H. W., 1961. "Stability of laminar flames". *Physics of Fluids,* ***4***(4), pp. 456–464.

[22] Baillot, F., Bourehla, A., and Durox, D., 1996. "The characteristics method and cusped flame fronts". *Combustion Science and Technology,* ***112***(1), pp. 327–350.

[23] Noiray, N., Durox, D., Schuller, T., and Candel, S., 2007. "Passive control of combustion instabilities involving premixed flames anchored on perforated plates". *Proceedings of the Combustion Institute,* ***31***(1), pp. 1283–1290.

[24] Kornilov, V., Rook, R., ten Thije Boonkkamp, J., and de Goey, L., 2009. "Experimental and numerical investigation of the acoustic response of multi-slit bunsen burners". *Combustion and Flame,* ***156***(10), pp. 1957–1970.

[25] Kornilov, V., Manohar, M., and de Goey, L., 2009. "Thermo-acoustic behaviour of multiple flame burner decks: Transfer function (de)composition". *Proceedings of the Combustion Institute,* ***32***(1), pp. 1383–1390.

[26] Duchaine, F., and Poinsot, T., 2010. "Sensitivity of flame transfer functions of laminar flames". *Center for Turbulence Research - Proceedings of the Summer Program.*